J Mater Sci (2011) 46:7012–7025
DOI 10.1007/s10853-011-5670-x

Liquid phase sintered Cu–In composite solders for thermal interface material and interconnect applications

J. Liu · P. Kumar · I. Dutta · R. Raj · R. Sidhu · M. Renavikar · R. Mahajan

Received: 13 February 2011 / Accepted: 30 May 2011 / Published online: 17 June 2011
© Springer Science+Business Media, LLC 2011

Abstract This study reports on the processing and characterization of composite solders produced by liquid phase sintering, which comprise a high-melting phase such as Cu embedded in a matrix of a low-melting phase such as In. These solders combine higher electrical/thermal conductivities with high mechanical compliance, and are suitable for a range of next-generation thermal interface material and interconnect applications. After considering a range of compositions, a solder with 60 volume percent In was found to possess the requisite combination of compliance and conductivity. A thin interfacial Au layer was utilized for the dual purposes of (a) enhancing the wetting between Cu and In, and (b) reducing interfacial reaction between Cu and In to form coarse intermetallic compounds (IMC) scallops, which adversely affect both mechanical and electrical/thermal properties. The Au layer increased the thermal conductivity of the solder by a factor of ~ 2 while reducing the yield strength to make the solder more compliant. The effects of particle size, shape, and volume fraction are discussed, and a simple model is utilized to explain the trends in the mechanical and the thermal properties.

J. Liu · P. Kumar · I. Dutta (✉)
School of Mechanical and Materials Engineering,
Washington State University, Pullman, WA 99164, USA
e-mail: idutta@wsu.edu

R. Raj
Department of Mechanical Engineering, University of Colorado,
Boulder, CO 80309, USA

R. Sidhu · M. Renavikar · R. Mahajan
Assembly Technology Development, INTEL Corporation,
Chandler, AZ 85226, USA

Introduction

With a continuous increase in the computational power and the miniaturization of the modern microelectronic devices, the requirements for heat dissipation via thermal interface materials (TIMs) and current density flow through chip-to-package interconnects (ICs) have drastically increased. Hence, the packaging of advanced next generation microelectronic devices demands development of solder alloys with (1) low melting temperature (2) low flow stresses in shear with moderate compressive stiffness under creep conditions, and (3) high electrical and thermal conductivities. To simultaneously attain the above characteristics in a solder, Dutta and co-workers [1–3] proposed a novel composite architecture, as shown in Fig. 1, composing of a highly conductive high melting phase (HMP, e.g., Cu, Sn, etc.) uniformly distributed in a highly complaint and soft low melting phase (LMP, e.g., In, etc.) matrix. This architecture proffers high thermal and electrical conductivities, which are controlled by the high conductivity HMP, along with low flow stresses in shear, which is controlled by the soft and compliant LMP. The considerable volume fraction of the hard HMP imparts good compressive strength to the solder. On the other hand, the low strain rate shear compliance of the solder joints prepared using these solders, which is critical for accommodating differential deformation between the chip and the heat-spreader (for TIM applications), or chip and substrate (for IC applications), can be quite high because of localization of strain in the continuous LMP network around the HMP particles during shear deformation [1–3]. Also, the reflow and the rework temperatures are controlled by the melting temperature of the LMP, which can be very low as compared to the existing Sn–Ag-based lead-free solders, making these composites suitable for low

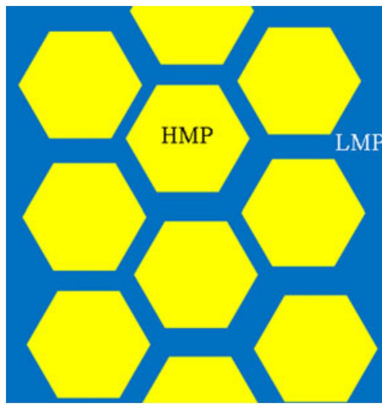

Fig. 1 Schematic of idealized LPS solder microstructure with a uniform distribution of HMP and LMP

temperature soldering, especially in fragile and heat-sensitive microelectronic packages.

Liquid phase sintering (LPS) is widely used for densification of hard-to-process and refractory materials, such as carbides, tungsten, and various ceramics to produce structural materials, high temperature bearings, piezoelectric materials, ferroelectromagnet materials, etc. [4–9]. Recently, LPS was also used to process materials for microelectronic packaging applications, such as solders, metal-polymer composites, etc., which contain a very low melting phase, such as In, polymers, etc. [1–3, 10–14]. Dutta and co-workers [1–3, 10] introduced LPS to produce Sn–In composites with short sintering times (1–2 min) at a temperature of 160–162 °C (just above the melting point of indium). By optimizing the In content, highly compliant Sn–In solders, with flow stresses close to that of pure In, were produced. The electrical and thermal conductivity of the LPS solder was found to be approximately half that of pure In. Based on a semi-empirical model [15], it was demonstrated that for a high conductivity HMP, LPS solders with very high thermal conductivity may be obtained so long as the HMP particle size is larger than a critical size (the Kapitza diameter), the advantage increasing with increasing thermal conductivity of the HMP. Hence, a composite system with Cu as the HMP and In as the LMP was chosen as a candidate LPS solder composite. Preliminary experiments on Cu–In showed [1, 2] that thermal conductivity of the composite solders were significantly greater than that of In, although the flow stress was high because of reactions between Cu and In, and the formation of a solid skeleton structure of the HMP and intermetallic compounds (IMCs) [1–3].

During LPS of a Cu–In composite, Cu and In react to form several IMCs at the Cu/In interface. The most common IMCs, which form in the temperature range of 160–175 °C, are $Cu_{16}In_9$ and $Cu_{11}In_9$ [16–18]. Since the Gibbs free energy of the formation of $Cu_{16}In_9$ (−7.58 kJ/mol [18]) is slightly more negative than that of $Cu_{11}In_9$ (−6.79 kJ/mol [18]), $Cu_{16}In_9$ IMC may preferentially form at the Cu-rich Cu–In interface in the beginning of the sintering process. However, once a thin continuous layer of Cu–In IMC is formed, the growth of the subsequent IMC layer is controlled by the diffusion of Cu through the IMC layer [17]. Since the activation energies for the growth of $Cu_{16}In_9$ and $Cu_{11}In_9$ layers are 59.5 kJ/mol and 16.9 kJ/mol, respectively [17], the growth rate of $Cu_{11}In_9$ in the later stages of sintering is much faster as compared to $Cu_{16}In_9$. The formed interfacial IMC layer continues to grow during thermal aging. During thermal aging at high temperature (>100 °C), CuIn may also form along with $Cu_{16}In_9$ and $Cu_{11}In_9$ [17]. However, the growth rate of $Cu_{11}In_9$ during isothermal aging is also much faster than that of other Cu–In IMCs [16] and hence the thickness of the interfacial IMC layer between Cu and In is thought to be primarily due to the growth of $Cu_{11}In_9$.

In general, the yield strength of LPS Cu–In composite solders is much greater than that of In due to the formation of IMCs at the Cu/In interface. However, as reported here, the reaction may be retarded by: (i) minimizing the total time available for reaction by minimizing the time spent at the sintering temperature, as well as the time spent above 125 °C following sintering (e.g., via rapid cooling from the sintering temperature), and (ii) utilizing a thin, deliberately produced reaction layer to serve as an interfacial barrier to continued inter-diffusion and reaction between Cu and In.

This article reports on the effects of: (i) the shape, size, and volume fraction of Cu particles, and (ii) an interfacial thin-film layer of Au (applied to the Cu particles as a surface deposit prior to sintering) on the electrical and thermal conductivity as well as the plastic flow behavior of LPS Cu–In composite solders with volume fraction of In varying between 50 and 80%. In addition, preliminary results on the microstructure and electrical properties of joints of Cu–In solders between Cu substrates are presented.

Experimental procedure

Composite solders, with Cu as HMP and In as LMP, were prepared via LPS for short times (1–2 min). Cu powders (either non-spherical or spherical), with average sizes of 1, 10, and 40 µm and 99.9% purity, were etched using 10% HCl solution for 10 min for removal of the native oxide layer. The etched powder was thoroughly rinsed using deionized water and dried by storing in vacuum (10^{-4} torr) for 12 h. An appropriate amount of Cu powder was mixed with 10 µm diameter, 99.99% purity In powder by vigorously shaking in a glass-vial. Mixing of powders and any subsequent short-term storage (<1 h) was performed in a glove box under dry-nitrogen atmosphere to prevent the oxidation of powders. Subsequently, the mixed powder was

uniaxially compressed in a lubricated hardened steel die to produce green pellets of 6 mm diameter and 1 mm height with a relative density of 90 ± 1%. All density measurements were conducted using Archimedes principle. The green pellets were encapsulated in Al foil, and liquid phase sintered at 160 °C by dipping them in pre-heated 200 mL silicone-oil bath for different lengths of time (15, 30, and 45 s), followed by quenching in water. Some of the sintered pellets were aged at 125 °C for 24 and 96 h to study the stability of the microstructure as well as the evolution in the mechanical, electrical, and thermal properties of the Cu–In solders. The sintered solder pellets were sectioned, and then mechanically polished with intermittent etching with 10% HCl solution up to a finish of 0.05 μm. The cross-sections were observed under a scanning electron microscope (SEM), using backscattered and secondary electrons (BSE and SE, respectively), as well as energy dispersive X-ray (EDX) spectroscopy.

To study the impact of an interfacial layer on the properties of the Cu–In solders, one more set of composite solders, with a thin interfacial layer of Au on Cu powders, was prepared following the same procedure as described above. Prior to powder mixing, Cu powders were coated with different thicknesses of Au layer (10, 50, and 200 nm). 10 and 50 nm of Au were deposited on Cu in one step using a commercially available direct immersion gold bath. 200 nm of Au coating on Cu was performed in two steps: (i) the first 50 nm was coated using direct immersion gold bath, and (ii) the rest of the coating was conducted using an electroless gold coating bath. Gold coated Cu powders were dried by placing them in high vacuum for 12 h. 1 and 10 μm Cu powders were coated with only 10 nm of Au layer whereas 40 μm Cu powders were coated with 50 and 200 nm of Au layer.

To further understand the formation and growth of IMC layer at the Cu/In and Cu(Au)/In interfaces, a few layered samples, comprising a 200 μm thick layer of In on a 3.12 mm thick Cu plate, with or without an interfacial layer of 200 nm thick Au layer, were also prepared. An etched In foil was placed on the Cu substrate (prepared by etching, followed by coating with Au as necessary), wrapped in Al foil, clamped, and then immersed in an oil bath at 165 °C for 90 s and subsequently cooled by water quenching. Cross sections of the layered samples were examined under SEM to study the extent of the IMC layer formation. Also, the In layer was dissolved by placing the sample in a 10% HCl solution for 12 h, to reveal the topography of the IMC layers. X-ray diffraction (XRD) was conducted on the etched surface to identify the IMCs formed at the Cu/In and Cu(Au)/In interfaces.

Mechanical properties of the solder were characterized using impression testing in a dynamical mechanical analyzer (DMA), using a 250 μm diameter cylindrical tungsten carbide punch. All tests were conducted at 25 °C at an equivalent uniaxial strain rate[1] of 3×10^{-4} s^{-1}. The thermal diffusivity (κ) of the samples was measured using a laser flash apparatus (LFA) and the specific heat (C_p) was measured using a differential scanning calorimeter (DSC), following which, the thermal conductivity (K) was determined as $K = \kappa C_p \rho_s$, where ρ_s is the density of the solder. The electrical resistivity of the composites was measured using a 4-wire Kelvin probe to eliminate the contact resistance.

A few joints of Cu(Au)–In composite solder and pure In between the ends of two 6 mm diameter Cu rods were made by placing the appropriate powder mix between the Cu rods in a modified mold, and then, uniaxially compressing to produce a green joint, which was subsequently sintered at 165 °C for 45 s. The joints were inspected metallographically, as well as characterized electrically.

Results and discussion

Effect of Cu particle shape

Figure 2 shows representative microstructures of the liquid phase sintered Cu–In composite solders with non-spherical and spherical particles. Both mixing and wetting were adequate, as evident from the complete penetration of liquid In between all Cu particles. The sintered density of all composites was ~97% and a few scattered pores were always present. Figure 2 shows much less IMC as compared to that reported in Ref. [1, 2], and this is attributed to the improved LPS processing conditions (primarily the reduced sintering and cooling times).

Figure 3 demonstrates the impact of Cu-particle shape on the strain response of the composite solder containing 50 volume percent In during impression testing. All the stress–strain plots are for uncoated Cu particles. Clearly, when the Cu particles are non-spherical, the yield strength of the solder is much greater than that for spherical particles at all test temperatures. This is largely attributable to the greater propensity for mechanical interlocking of adjacent Cu particles during extensive plastic flow of the intervening In, although some of it may also be due to the greater IMC volume fraction produced due to the larger interfacial area associated with non-spherical particles. Since an important goal of this study is to produce soft, pliable microstructures, it is apparent from the above that the Cu particles must be spherical for these composites to be suitable for the proposed TIM and IC applications.

[1] Equivalent uniaxial strain rate is equal to $\dot{\delta}/\phi$, where $\dot{\delta}$ is the displacement rate of the punch and ϕ is the diameter of the punch [19].

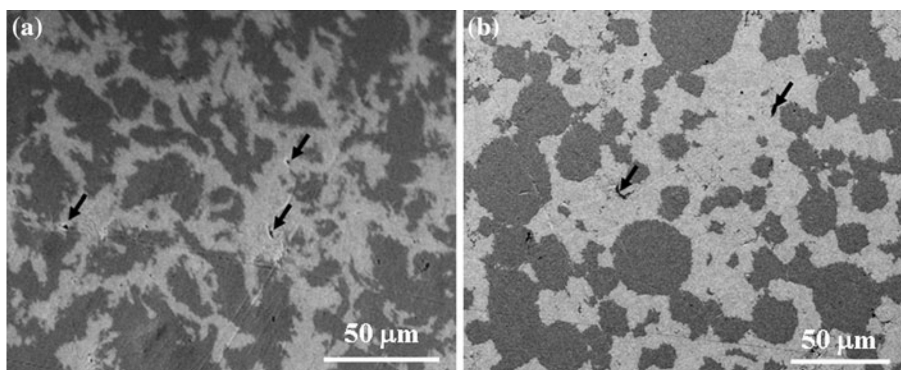

Fig. 2 SEM micrographs showing the cross-section of **a** non-spherical Cu-50 vol% In and **b** spherical Cu-50 vol% In composite solders. The solders were sintered at 160 °C for 45 s. The *dark areas* represent Cu and the *light areas* represent In. *Arrows point* to some of the pores

Hereafter, all solders that are reported in this study were prepared using only spherical Cu powders.

Effect of Indium volume fraction

Figure 4 shows the effect of volume fraction of In on the electrical resistivity and the yield strength of the Cu–In composite solders. As shown in Fig. 4, an increase in the volume fraction of In increased the electrical resistivity of the solders, which can be attributed to the replacement of high conductivity phase, Cu, with the poor conductivity phase, In. The trend shown in Fig. 4 is consistent with an earlier reported semi-empirical model that predicts a monotonous decrease in the thermal conductivity of a composite with an increase in the lesser conductive constituent [1, 3]. Since electrons are the major carriers of the electric current as well as the thermal energy in metallic materials, variation in the thermal conductivity of a metallic material due to a stimulus is analogous to the variation in its electrical conductivity.

Figure 4 also shows that: (i) when the In volume fraction is relatively small, the yield strength of the Cu–In solders decreases rapidly with the In volume fraction, and (ii) at high volume fraction of In ($\geq$60%), the yield strength of the solders shows saturation. Since most of the strain in the Cu–In solders is localized in the In matrix, the yield strength of the solder should be determined by the yield strength of In. Since Cu particles act as nucleation sites for the In grains, the Cu particle volume fraction may affect the yield strength of In via Hall–Petch relationship [20]. However, yield strength data at high In volume fraction, as shown in Fig. 4, suggests that the effect of Cu particle volume fraction on the In grain size (or, Hall–Petch relationship) in these Cu–In solders is insignificant and can be neglected. An incremental increase in the yield strength of

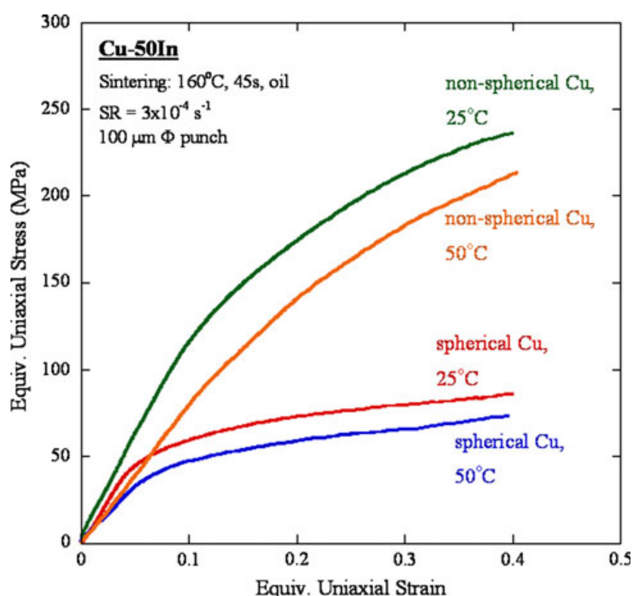

Fig. 3 A few representative stress–strain plots showing the effect of particle shape on the strain response of the as-sintered solders containing 50 vol% In

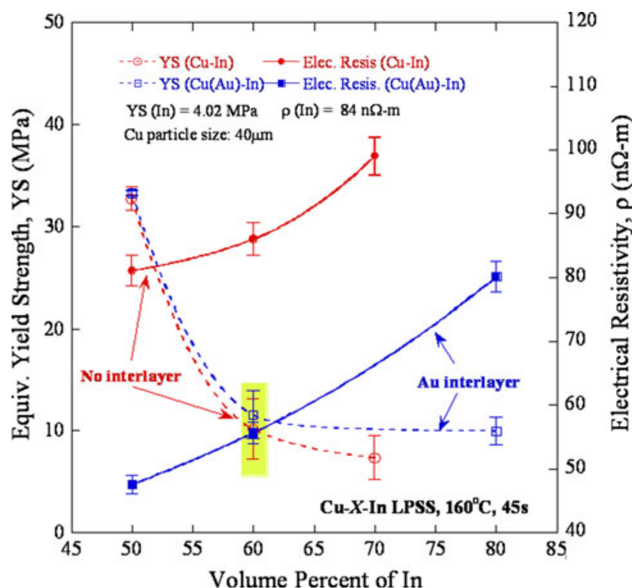

Fig. 4 Variation in the yield strength and the electrical resistivity of the Cu–In-based solders with In volume fraction. The *shaded* region in the plot shows a sweet spot where both optimum yield strength and electrical resistivity can be achieved

the composite can be induced by an increase in the dislocation density in In, which may occur due to: (i) the coefficient of thermal expansion (CTE) mismatch between the reinforcement particle (Cu) and the matrix (In) [20–22], and (ii) the geometrical mismatch between the elastically deforming reinforcement particles and the plastically deforming matrix [23, 24]. The dislocation density is highest next to the particles, and decreases rapidly with the distance from the interface [22]. Hence, the effects of the above two interface-based dislocation sources on the strengthening of the composites become relevant only when the inter-particle spacing (i.e., In channel width between two Cu particles) is small. In addition to the strengthening due to dislocations, concurrent recovery mechanisms which tend to soften the matrix during testing also operate. The observed yield strength of the composite thus depends on the superposition of these two effects (i.e., hardening due to dislocations and creep). These effects are quantified below.

The increase in yield strength due to thermally induced dislocations is given by [21]:

$$\Delta\sigma_{CTE} = \alpha_1 G\sqrt{\frac{Bb\Delta T\Delta\alpha}{d}\frac{(1-V_{\mathrm{m}})}{V_{\mathrm{m}}}} \quad (1)$$

where V_{m} (=1−V_{r}) is the volume fraction of the matrix, V_{r} is the volume fraction of reinforcement particles, ΔT is the temperature difference between the heat treatment temperature of the composite and room temperature, $\Delta\alpha$ is the mismatch between CTEs of the particles and the matrix, b is the Burger's vector of matrix, G is the shear modulus, α_1 is a constant used in the Orowan equation ($\Delta\sigma = \alpha_1 Gb\sqrt{\rho}$, where $\Delta\sigma$ is the incremental increase in the yield strength, and ρ is the dislocation density), B is a geometrical factor, which is equal to ~12 for cubic particles, and d is the particle diameter. The incremental strengthening due to strain mismatch induced plasticity (i.e., geometric mismatch) is given by [23, 25]:

$$\Delta\sigma_{geo} = K_1 G\sqrt{\frac{b\varepsilon(1-V_{\mathrm{m}})}{d}} \quad (2)$$

where K_1 is a dimensionless constant with typical values ranging from 0.2 to 0.4 [23], and ε is the applied normal strain. Using $B = 12$, $\Delta T =$ sintering temperature–room temperature = 135 K, $\Delta\alpha = \alpha_{\mathrm{In}}-\alpha_{\mathrm{Cu}} = 1.5 \times 10^{-5}$ K^{-1} and assuming $\alpha_1 \sim 1$, $K_1 = 0.4$ [25] and $\varepsilon\sim$ the plastic strain at the yield strength = 0.002, the increase in the yield strength due to CTE mismatch, as predicted by Eq 1 will be at least 1 order of magnitude larger than that due to the geometrical mismatch, as predicted by Eq. 2, for the volume fraction of matrix (In) used in this study. Hence, Eq. 1 adequately predicts the increment in the yield strength of the Cu–In-based composite solders.

In a particle reinforced composite with a very soft and compliant matrix (such as In), the contribution of load transfer to composite strengthening is negligible, and the composite yield strength σ_{cy} equals the matrix yield strength σ_{my}. Immediately following fabrication (prior to any stress relaxation), the 'initial' composite yield strength $\sigma_{\mathrm{cy,i}}$, is given by:

$$\sigma_{\mathrm{cy,i}} \approx \sigma_{\mathrm{my,o}} + \Delta\sigma_{\mathrm{CTE}} \quad (3)$$

where $\sigma_{\mathrm{my,o}}$ is the yield strength of the annealed matrix (In).

In a particulate-reinforced composite with a soft matrix, the matrix and reinforcement particles are nominally in iso-stress (i.e., $\sigma_{\mathrm{m}} = \sigma_{\mathrm{r}}$, where the subscripts m and r represent the matrix and particles, respectively), and the strain is partitioned based on the respective volume fractions (V_{m} and V_{r}), as follows:

$$\varepsilon_{\mathrm{c}} = \varepsilon_{\mathrm{m}}\mathrm{V_m} + \varepsilon_{\mathrm{r}}\mathrm{V_r} \quad (4)$$

where ε_{c}, ε_{m}, and ε_{r} are strains in the composite, the matrix, and the reinforcement, respectively. During the time that elapses during testing, the In matrix, for which ambient temperature corresponds to ~70 percent of the melting temperature, undergoes stress relaxation by creep, and

$$\frac{\mathrm{d}\varepsilon_c}{\mathrm{d}t} = V_m\frac{\mathrm{d}\varepsilon_m}{\mathrm{d}t} + V_r\frac{\mathrm{d}\varepsilon_r}{\mathrm{d}t} \quad (5)$$

where ε_{r} is elastic, and ε_{m} has both elastic and plastic components. At a fixed applied strain ($\mathrm{d}\varepsilon_{\mathrm{c}}/\mathrm{d}t = 0$), the rate of increase of time-dependent matrix plastic (i.e., creep) strain $\varepsilon_{\mathrm{mp}}$ is balanced by the rate of decrease of the elastic strain components $\varepsilon_{\mathrm{me}}$ and ε_{r} (and hence the associated stress $\sigma_{\mathrm{m}} = \sigma_{\mathrm{r}}$), as follows:

$$V_m\left(\frac{1}{E_{\mathrm{m}}}\frac{\mathrm{d}\sigma_m}{\mathrm{d}t} + C\sigma_{\mathrm{m}}^n\right) = -\frac{V_r}{E_r}\frac{\mathrm{d}\sigma_r}{\mathrm{d}t} \quad (6)$$

where E_{m} and E_{r} are the Young's modulus of the matrix and reinforcement, respectively, C is the creep constant (=A.(Gb/kT).e$^{-Q/RT}$, where A is the Dorn constant, Q is the activation energy for creep of the In matrix, R is the gas constant, and T is the temperature), and n is the creep exponent for the In-matrix.

Realizing that at time $t = 0$, the initial matrix stress is $\sigma_{\mathrm{m,i}}$, integrating Eq. 6 yields:

$$\sigma_{\mathrm{m}} = \left[\sigma_{\mathrm{m,i}}^{-(n-1)} + (n-1)V_{\mathrm{m}}E_{\mathrm{c}}^{'}C\frac{\varepsilon}{\dot{\varepsilon}}\right]^{-\frac{1}{n-1}} \quad (7)$$

where $\varepsilon/\dot{\varepsilon}$ is the ratio of applied strain to strain rate, and represents the elapsed time t, and $1/E_{\mathrm{c}}' = V_{\mathrm{m}}/E_{\mathrm{m}} + V_{\mathrm{f}}/E_{\mathrm{f}}$. As the matrix stress relaxes, the rearrangement of dislocations also leads to a decrease in the matrix yield strength, and therefore, the composite yield strength. Thus,

Eq. 7 may also be used to describe the instantaneous yield strength, as follows:

$$\sigma_{cy} = \left[\sigma_{cy,i}^{-(n-1)} + (n-1)V_m E_c' C \frac{\varepsilon_c}{\dot{\varepsilon}}\right]^{-\frac{1}{n-1}} \tag{8}$$

Combining Eqs. 1, 3, and 8 gives, for the composite flow stress at any applied strain ε_c:

$$\sigma_{cy} = \left[\left(\sigma_{my,o} + \alpha_1 G\sqrt{\frac{Bb\Delta T\Delta\alpha}{d}\frac{(1-V_m)}{V_m}}\right)^{-(n-1)} + (n-1)V_m E_c' C \frac{\varepsilon_c}{\dot{\varepsilon}}\right]^{-\frac{1}{n-1}} \tag{9}$$

Figure 5 shows a plot of Eq. 9 for a Cu–In composite at two strain rates. At the lower strain rate, the creep component is overestimated by Eq. 9, since the assumption of $d\varepsilon_c/dt = 0$ overestimates the constraint imposed on the matrix by the reinforcements, leading to an over-estimation of the extent of matrix stress relaxation. At higher V_m values, the stress-relaxation predicted is somewhat more accurate. Therefore, the actual yield behavior is expected to transition from the higher strain rate curve at low V_m to the lower strain rate curve at high V_m. The result thus provides insight into the observed experimental trend (Fig. 4) that the yield strength decreases steadily with increasing V_m until ~60 vol.% In, and then levels off at higher V_m values because of rapid stress-relaxation. Thus, despite the limitations associated with the assumption of iso-stress condition (and the associated difficulties in predicting strain/stress partitioning and stress relaxation), Eq. 9 provides a reasonable first approximation of the yield strength, including creep effects.

For TIM and IC applications, a solder is required to possess both low electrical/thermal resistivity and high compliance. As shown in Fig. 4, these two traits go in opposite directions with In volume fraction. Hence, optimization with respect to the In volume fraction should be conducted to achieve acceptable values for both electrical/thermal conductivity and the yield strength for a particular application. An optimum volume fraction of In for TIM and IC applications was determined to be 60% for Cu-In solders. At this composition, Cu–In composite solders showed a similar electrical/thermal conductivity as of pure In with only ~2 times increase in the yield strength as compared to pure In.

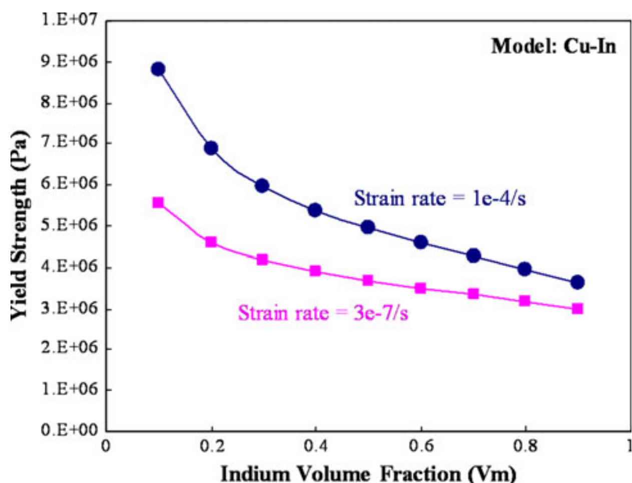

Fig. 5 Variation in the yield strength of Cu–In composite solders with matrix volume fraction, as predicted by Eq. 9, at two strain rates

Effect of sintering time and temperature

Figure 6a, b shows the effect of sintering conditions on the extent of densification during LPS for both non-spherical and spherical particles. With increase in the green density of the pellet, the sintered density increases, as expected. However, it is readily apparent from the plots that the extent of densification during sintering is very limited under most conditions (only ~2–5% densification beyond the green density). This is true irrespective of the type of sintering treatment rendered (sintering in oil or N_2 environment), despite the fact that microstructural observation reveals nearly fully dense microstructures, with minimal porosity. Clearly, some artifact in the microstructure tends to reduce the sintered density, especially when the overall exposure time to high temperatures (above ~125 °C) is long (>2 min), as in these samples (which were sintered for <2 min at ≥160 °C, but cooled slowly enough to spend 1–2 min more above 125 °C).

Figure 7a, b shows the effects of sintering time and temperature on the sintered density more clearly. From Fig. 7a, it is apparent that a shorter sintering time (45 s) produces a greater density than a longer time (60 s). But confoundingly, an increase in In content also reduces density. Figure 7b shows that a higher sintering temperature (beyond ~162 °C) also reduces density, although the density rises at 170 °C for longer sintering and cooling times. As noted previously and shown in Fig. 8 via X-ray diffraction spectrum of Cu/In interface, a series of interfacial IMCs may form during sintering and subsequent cooling, depending on the time of exposure of the Cu to molten In during LPS, as well as solid-state reactions occurring during cooling. The IMCs formed include CuIn[2], $Cu_{11}In_9$, and $Cu_{16}In_9$ (or η), which have densities of 7.656×10^3 [26], 8.614×10^3 [27] and 7.676×10^3 kg/m^3 [28][3], respectively, as compared to In and Cu which

[2] Even though CuIn is not shown in standard phase diagrams, its existence in Cu–In systems has been widely reported in literature, for example in Ref. [26, 27].

[3] $Cu_{16}In_9$ exists in two crystallographic forms, whose densities are 8.244 x 10^3 and 7.676 x 10^3 kg/m^3, respectively; however, only the latter is stable at temperatures relevant to this study [29].

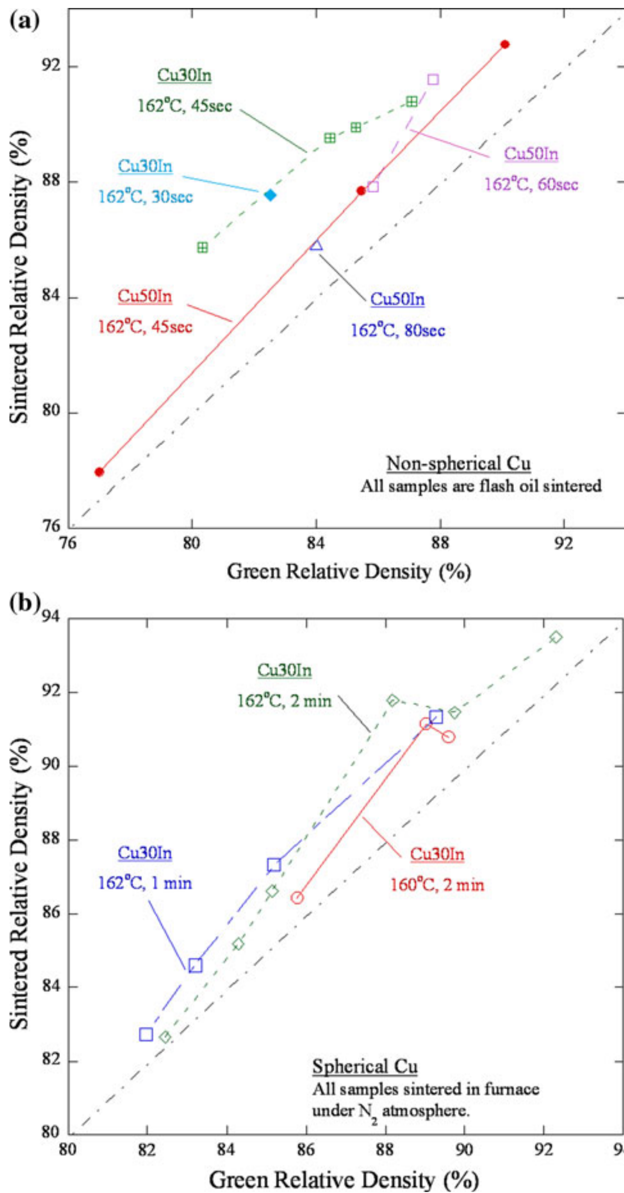

Fig. 6 The effect of sintering conditions on the extent of densification during LPS for both non-spherical and spherical particles

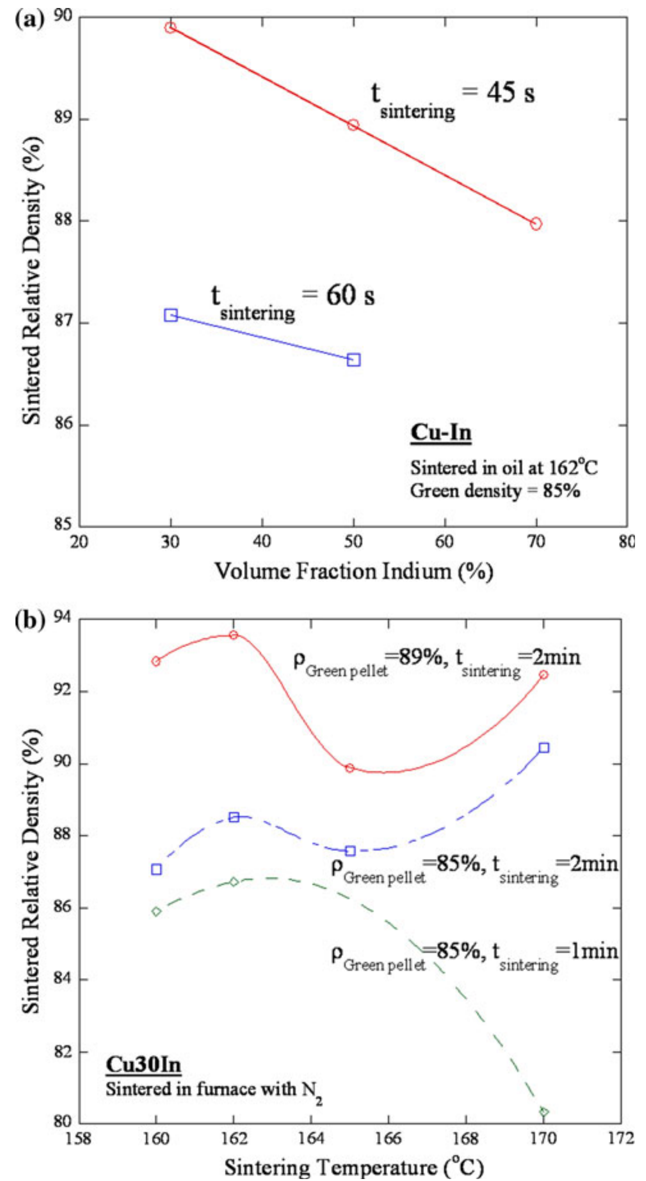

Fig. 7 The effect of **a** volume fraction of In and **b** sintering temperature on the sintered relative density of the Cu–In solders

have densities of 7.31×10^3 and 8.96×10^3 kg/m^3, respectively. Thus, the formation of CuIn and $Cu_{16}In_9$ produces a decrease in density relative to the unreacted Cu–In composite, whereas the formation of $Cu_{11}In_9$ causes an increase. As sintering occurs, and these reaction products are formed in sequence, and as a result, the apparent relative density may decrease even as pores are eliminated due to the sintering. For example, as explained earlier, $Cu_{16}In_9$ forms preferentially at the beginning of the sintering and $Cu_{11}In_9$ forms predominately only after a thin continuous IMC layer is formed around Cu particles; hence, the sintered density of the solders decrease with sintering time in the beginning (Fig. 7a) and increase with sintering time at longer sintering times (Fig. 7b). A greater amount of liquid In facilitates greater intermetallic growth, and therefore a larger apparent reduction in relative density as noted in Fig. 7a.

Importantly, it is apparent from the above discussion that the as-sintered relative density reflects not just the pore-content of the composite solder, but also the amount and type of intermetallics formed. Indeed, as revealed by the nearly fully dense microstructure, densification to 95–97% relative density can occur within a short time (<45 s of LPS at 160 °C), and this density can be maintained as long as the solder is cooled rapidly.

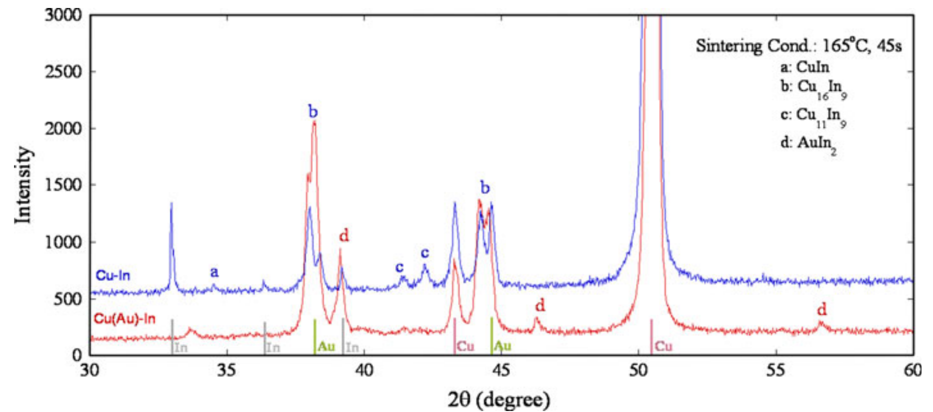

Fig. 8 XRD spectrum from Cu–In and Cu(Au)–In layered samples showing the relevant IMC phases formed during reflow at 165 °C for 45 s. The In layer was etched away using 10% HCl solution. The upper spectrum corresponds to Cu–In sample whereas the lower one corresponds to Cu(Au)–In. Peaks corresponding to IMC phases are marked with *lower-case alphabets*

Interfacial reaction and role of Au barrier layer

As-sintered condition

Figure 9a, b shows the cross section of the layered samples without and with Au interfacial layers, respectively. In both types of layered samples, a continuous layer of IMCs was formed at the interface between In and Cu. However, a 200 nm of Au layer on Cu drastically reduced the total thickness of the interfacial IMC layer from ~22 to ~8 µm. This clearly demonstrates the effectiveness of the Au as a diffusion barrier between In and Cu. Figures 9c, d shows the morphology of the IMC layer formed over Cu substrate, without and with Au layer, respectively, as revealed after the removal of In. As shown in Fig. 9c, d, all IMCs were faceted with preferred planes of growth; however, the IMCs formed over Au-coated Cu substrate were significantly finer as well as shorter than the IMCs formed over bare Cu substrate. As shown in Fig. 8, XRD analysis of the surfaces revealed that the majority of the IMC formed over bare Cu substrate were $Cu_{16}In_9$ and $Cu_{11}In_9$ whereas $AuIn_2$ and $Cu_{16}In_9$ IMCs formed over Au-coated Cu substrate. The presence of the IMCs here are consistent with the equilibrium phase diagrams [18, 30, 31] and the earlier reports on Cu–In [16, 17] and Au–In [32] systems. The reported kinetic data on the growth of above IMCs [17, 32] suggests that the growth kinetics of $Cu_{11}In_9$ is the fastest whereas $Cu_{16}In_9$ grows at the slowest rate at 160 °C, which is consistent with Fig. 9. Summarily, the following two can be inferred from this discussion: (i) once a thin layer of $Cu_{16}In_9$ forms over bare Cu substrate, $Cu_{11}In_9$ forms whose growth is rapid as well as scallopy, and (ii) in the presence of a thin interfacial layer of Au, first, a very thin layer of $AuIn_2$ forms quickly at the Cu substrate,[4] which then acts as an effective diffusion barrier between Cu and In and impedes the formation of Cu–In IMCs.

Figure 10 shows the cross-section of composite solders, without and with Au interfacial layer, sintered for only 15 s. Even at this short sintering time, the solder with Au interfacial layer attained a sintered density of ~95% with much less fraction of porosity as compared to the solder without Au interfacial layer. This proves that Au interfacial layer also substantially improved the wetting between Cu and In. This is attributed to the very good wetting between In and Au [32].

Figure 4 compares the effect of Au interfacial layer on the yield strength and electrical resistivity of the as-sintered solders. Both kinds of solders show similar trends, in the yield strength and electrical resistivity with the In volume fraction. Figure 4 shows that the difference in the yield strength between as-sintered Cu–In and as-sintered Cu(Au)–In solders was insignificant. Since most of the plastic deformation was concentrated in the soft matrix, whose volume fraction did not change during short-time sintering, and the difference in the thicknesses of the IMC layers in Cu–In and Cu(Au)–In solders were much smaller than the Cu particles (Fig. 11a, c), the effect of Au coating on the yield strength of the solder was insignificant. However, as shown in Fig. 4, the electrical resistivity of Cu(Au)–In solders was significantly smaller than that of Cu–In solders. This can be attributed to the lower contact resistance of Cu(Au)/In interface as compared to that of Cu/In interface. The contact resistance depends on the wetting and the conductivity of the interfacial IMC layer. Since (i) wetting between In and Au-coated Cu is significantly better than that between In and Cu, and (ii) the electrical resistivities of $AuIn_2$ and $Cu_{11}In_9$ are 78 [33] and 170 nΩ-m [34], respectively, the contact resistance of Cu(Au)/In interface is much smaller than Cu/In interface. Similar to Cu–In solders, 60 vol.% In gives optimum properties for the Cu(Au)–In solders also. At this In volume fraction, Cu(Au)–In composite solders showed ~1.5 times higher electrical/thermal conductivity as compared to

[4] Owing to much more negative Gibbs free energy of formation of $AuIn_2$ (−21.317 kJ/mol at 160 °C [32]), this IMC forms rapidly when liquid In comes in contact with the interfacial Au layer.

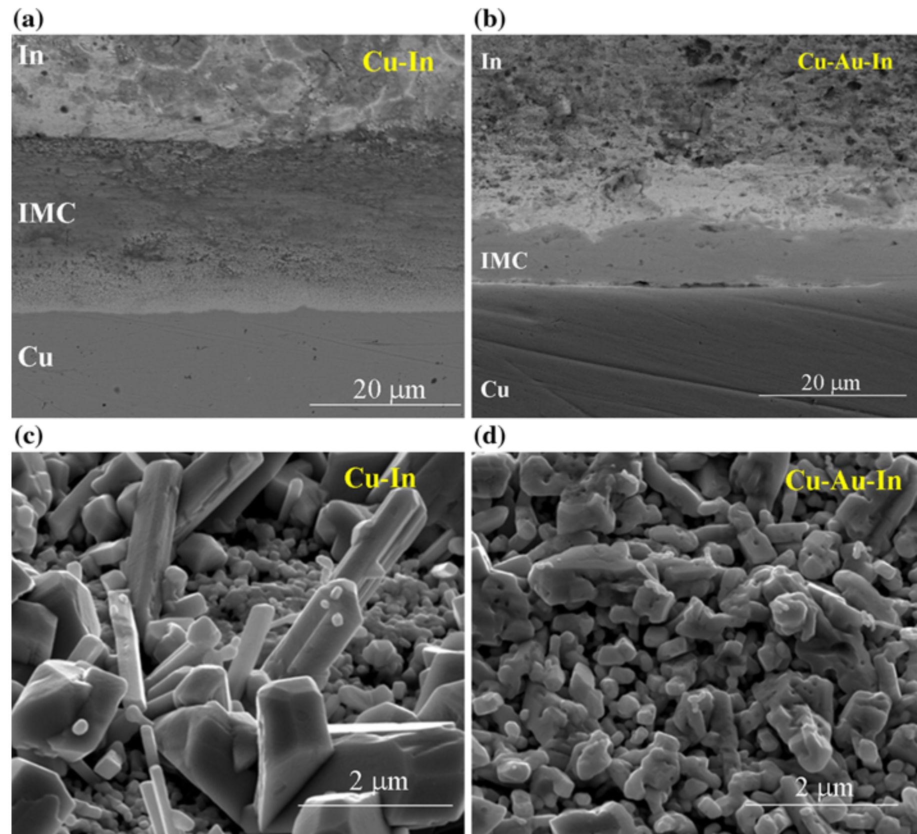

Fig. 9 Cross-sectional micrographs of the interfaces, showing continuous layers of IMCs at **a** Cu/In interface, and **b** Cu/200 nm Au/In interface. In was then etched away revealing the IMC morphology at the Cu/In interface: **c** bare Cu substrate and **d** 200 nm Au-coated Cu substrate. All micrographs correspond to the as-reflowed condition

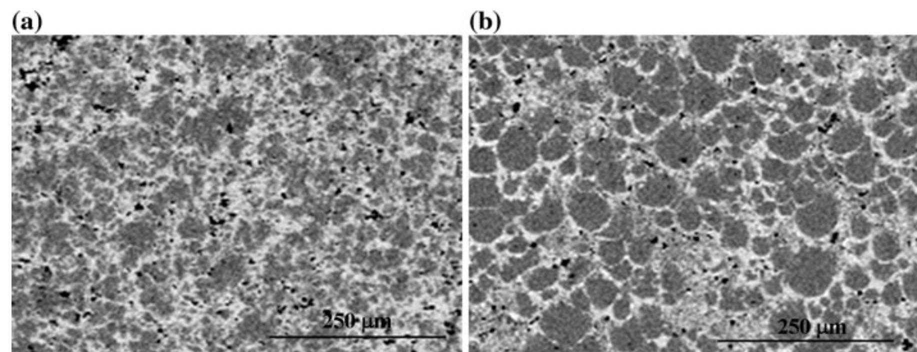

Fig. 10 Microstructures of as-sintered **a** Cu–In and **b** Cu(Au)–In solders, sintered at 160 °C for 15 s. The *black* regions show pores

In (and Cu–In solder) and only ~2 times higher yield strength as compared to pure In.

Effect of isothermal aging

Solders, in both TIM and IC applications, are exposed to elevated temperatures during service that may cause microstructural evolution in Cu–In-based solders and deteriorate their mechanical, electrical, and thermal properties. Hence, aging study was conducted to evaluate the effect of the microstructural evolution on the mechanical and electrical properties of the Cu–In and Cu(Au)–In solders. Figure 11 shows the effect of isothermal aging on the Cu–In and Cu(200 nm-Au)–In composite solders. Figure 11a shows formation of a very thin layer of IMC at the Cu/In interface, which becomes apparent only at high magnification. However, as shown in Fig. 11b, the Cu–In IMCs in Cu–In solders thickens very rapidly with aging resulting in a few very small isolated zones of unreacted In. On the other hand, $AuIn_2$ IMC forms very rapidly during the LPS of Cu(Au)–In solders (Fig. 11c), and remains tenaciously intact during the aging allowing only limited diffusion of In through it. This results in the formation of Cu–In IMC in between the “protective ring” of the $AuIn_2$ IMC and the Cu particles (Fig. 11d), leaving large regions of unreacted In in the Cu(Au)–In solder matrix.

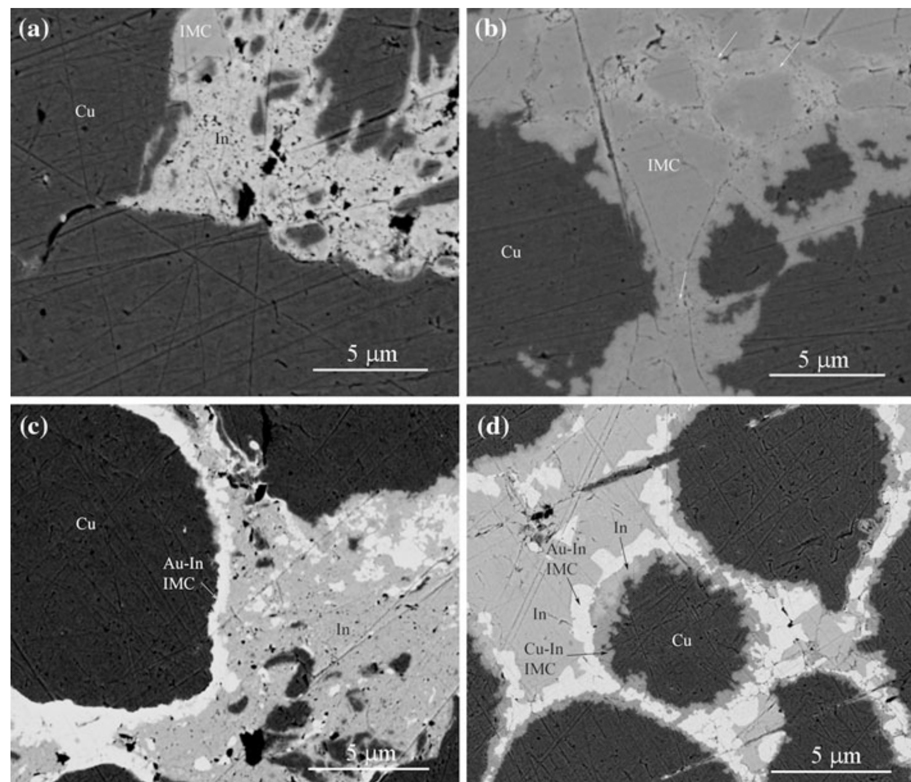

Fig. 11 Microstructures of the solders with different aging conditions. **a** As-sintered Cu–In, **b** Cu–In solder after an aging for 96 h, **c** As-sintered Cu(200 nm Au)–In, **b** Cu(200 nm Au)–In solder after an aging for 96 h. The *arrows* in (**b**) show the isolated regions of unreacted In

Figure 12 shows the effect of aging on the yield strength and the electrical resistivity of Cu–In and Cu(Au)–In solders. The yield strength and the electrical resistivity of the composite solders monotonically increased with aging. This can be attributed to the growth of the IMC layer at the Cu/In and Cu(Au)/In interfaces, as shown in Fig. 11. In the beginning, the increases in the yield strength as well as the electrical resistivity were very steep due to a corresponding steep increase in the IMC thickness (IMC thickness $\propto t_{\text{aging}}^{0.5}$, where t_{aging} is the aging time [17, 32]). With increase in the aging period, the growth in the IMC layer slows down [17, 32], resulting in a similar trend in the yield strength and electrical resistivity of the solders also. As discussed earlier that the Au interfacial layer acts as an effective diffusion barrier layer, the IMC growth kinetics in the Cu(Au)–In solders was much slower than that in Cu–In. Thus, the microstructure and hence the relative evolution in the mechanical and the electrical properties of Cu(Au)–In solder was slower than that of Cu–In solders.

Effect of Au-layer thickness

Figure 12 shows that the impact of the thickness of Au layer on the yield strength of the solder in the as-reflowed and aged conditions is less pronounced; however, a composite with thicker interfacial Au layer distinctively showed lower electrical resistivity for all aging conditions. As stated earlier and shown in Fig. 11, the $AuIn_2$ IMC forms almost instantaneously during LPS (or reflow), consuming all available Au, and then acts as a tenacious diffusion barrier layer between Cu and In. Since the difference in the thicknesses of Au layer between the two Cu(Au)–In composites (150 nm) is insignificant in comparison to the size of the Cu particles (40 μm) and the average channel width between Cu particles (~50 μm), the effect of Au layer thickness has insignificant effects on the volume fraction of unreacted In, resulting in similar yield strength behavior at all thicknesses of Au layer. On the other hand, a thicker layer of Au insures continuous conformal coating of Cu powders, which also has higher probability of remaining unbroken during powder mixing and compaction of mixed powders. Also, a thick interfacial layer of ductile Au can endure plastic deformation to accommodate the differential thermal expansion ($\alpha_{Cu} = 1.65 \times 10^{-3}$ and $\alpha_{Au} = 1.42 \times 10^{-5}$/K) during the rapid heating of the mixed powders and hence a fewer micro-cracks will form in the thick Au interfacial layer as compared to a thin one. Hence, the overall wetting between Cu and In as well as the effectiveness of Au layer in inhibiting the Cu–In IMC formation improve with thickening of Au layer leading to the reduction in the contact resistance. Also, an increase in the thickness of highly conductive $AuIn_2$ IMC layer (electrical resistivity = 78 nΩ-m [33]) on the expense of In (electrical resistivity = 84 nΩ-m [34]) will also result in an overall lower conductivity for the Cu(Au)–In solder with higher thickness of Au layer.

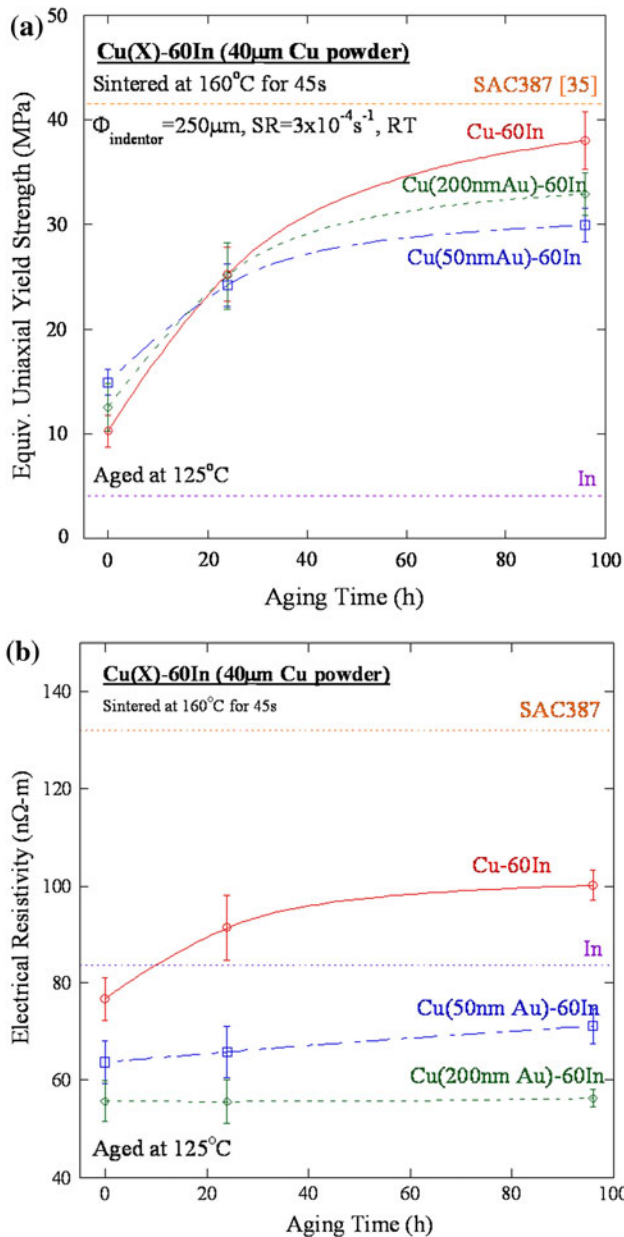

Fig. 12 Effect of aging on **a** the yield strength, and **b** the electrical resistivity of composites made with 40 μm Cu particles coated with *different thicknesses* of Au

Figure 12 also shows the yield strength and the electrical resistivity of commonly used lead-free Sn-3.8%Ag-0.7%Cu (SAC387) solder. It is noteworthy that the yield strength as well as the electrical resistivity of both Cu–In and Cu(Au)–In solders remain lower than that of SAC387, even after severe aging. This certainly justifies the use of Cu–In-based composite solders in IC applications, especially where a soft solder is required. This is of particular advantage owing to the low reflow or reworking temperature of these solders as compared to SAC 387 or other Sn–Ag-based solders.

Effect of Cu particle size on Cu(Au)–In solders

Figure 13 shows the effect of particle size of Cu on the yield strength and the thermal conductivity of Cu(Au)–In solders with 60 vol% In. By decreasing the particle size of Cu from 40 to 1 μm, the yield strength of the solder increased by ∼3 times and the thermal conductivity decreased by ∼20%. Figure 4 shows that 60 vol% In is near the limit below which the interfacial strengthening effects become significant. Since the interfacial area increases and the In channel width (i.e., inter-particle spacing) decreases with the particle diameter, the interfacial strengthening effects will be significant in Cu(Au)–60 vol% In solders with smaller Cu particles. Hence, Eqs. 1 and 9 can be used to explain the dependence of the yield strength on the size of Cu particles.

A decrease in the thermal conductivity with an increase in the particle size, as shown in Fig. 13, is attributed to a decrease in the total interfacial/contact area between Cu and In with an increase in the particle size. This behavior can be explained as follows: The thermal contact resistance of a solder can be calculated as follows [1–3]:

$$R_c^{th} = \frac{d}{2V_{Cu}}\left(\frac{1}{K_{meas}} - \frac{V_{Cu}}{K_{Cu}} - \frac{V_{In}}{K_{In}}\right) \tag{10}$$

where R_C^{th} is the thermal contact resistance, V_{Cu} and V_{In} are the volume fraction of Cu and In in the solder, respectively, and K_{meas}, K_{Cu}, and K_{In} are the measured thermal conductivity of the solder, thermal conductivity of Cu and In, respectively. The average value of the thermal

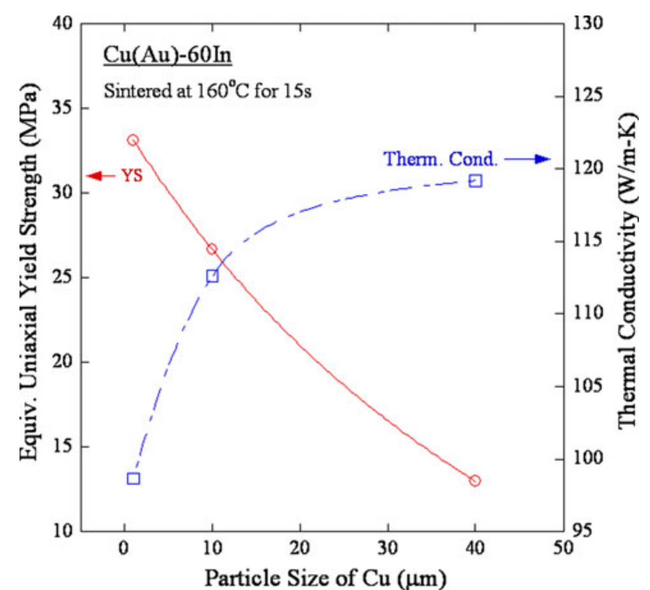

Fig. 13 Effect of particle size of Cu on the yield strength, and the thermal conductivity of composites with 60 vol% of In. All the samples were sintered at 160 °C for 15 s

contact resistance for the Cu(Au)–60 vol% In was calculated to be equal to $4 \pm 2 \times 10^{-9} m^2$ K/W. Now, this R_C^{th} value can be used in the following equation [1–3] to calculate the impact of the Cu particle size on the thermal conductivity of Cu(Au)–In solders:

$$V_{In}^3 = \left(\frac{1}{k}\right)^{\frac{1+2\alpha_t}{1-\alpha_t}} \left[\frac{k - r(1-\alpha_t)}{1 - r(1-\alpha_t)}\right]^{\frac{3}{1-\alpha_t}} \quad (11)$$

where α_t is the ratio of the Kapitza radius to the radius of the HMP (i.e., $\alpha_t = 2a_K/d$, where a_k is the Kaptiza radius defined as $a_k = R_C^{th} K_{In}$), k is the ratio of thermal conductivity of the solder to that of the LMP ($k = K_{solder}/K_{In}$) and r is the ratio of the thermal conductivity of the HMP to that of the LMP ($r = K_{HMP}/K_{LMP}$). Figure 14 shows the variation in the thermal conductivity of solder with particle size of the Cu, as predicted by Eq. 11. Irrespective of the thermal contact resistance, the thermal conductivity of the solder increases with the particle size of Cu, which is consistent with the experimental data as shown in Fig. 13. Interestingly, when the composite has a higher thermal contact resistance, the particle size has a significant effect on the thermal conductivity of the solder. If the thermal contact resistance, which depends on the wetting, and the thickness and composition of the interfacial IMCs, is sufficiently low, the composite prepared with even much smaller Cu powders (e.g., 1 μm) can show very high thermal conductivity. In addition to sintering procedure followed in this study, the thermal contact resistance of the powders can further be reduced by improving powder mixing process so that agglomeration of Cu powders, which is a major problem associated with fine Cu powders, is prohibited. This will reduce the fraction of pores formed in between the solid Cu powders.

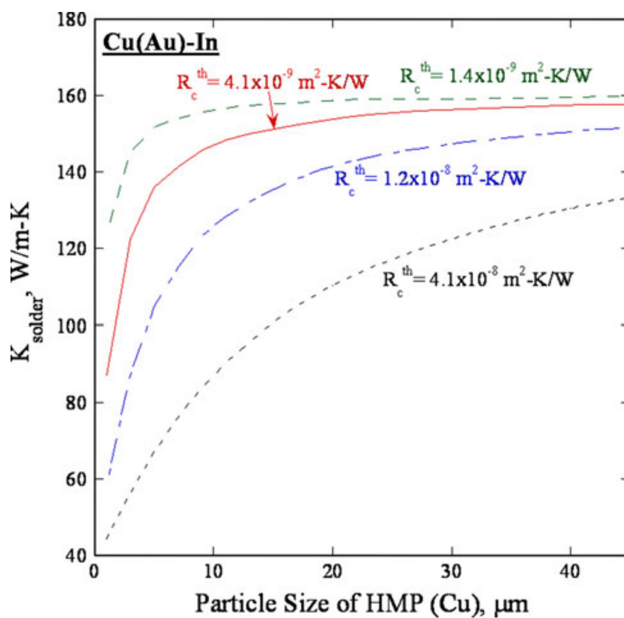

Fig. 14 A parametric study showing the effect of the particle size of Cu on the thermal conductivity of the solder, for various thermal contact resistances

Solder joints with Cu(Au)–In solders

Figure 15 shows a LPS solder joint formed between two Cu rods of 6 mm diameter. The solder was made of 40 μm Cu coated with a 50 nm thick layer of Au. Figure 15b shows a SEM micrograph of the interfacial region, revealing the presence of an IMC layer at the interface. This confirms that the joint interfaces were chemically well-bonded.

The joint electrical resistance was measured using 4-wire method. The electrical resistance of a joint with Cu(Au)–In solder was found to be 1.92 μΩ. Joint resistance of another sample with the same joint thickness (0.61 mm) and cross-section area, but prepared using pure In, was also measured. The resistance of the joint with pure In was 2.65 μΩ, which is almost ~1.4 times as that of the

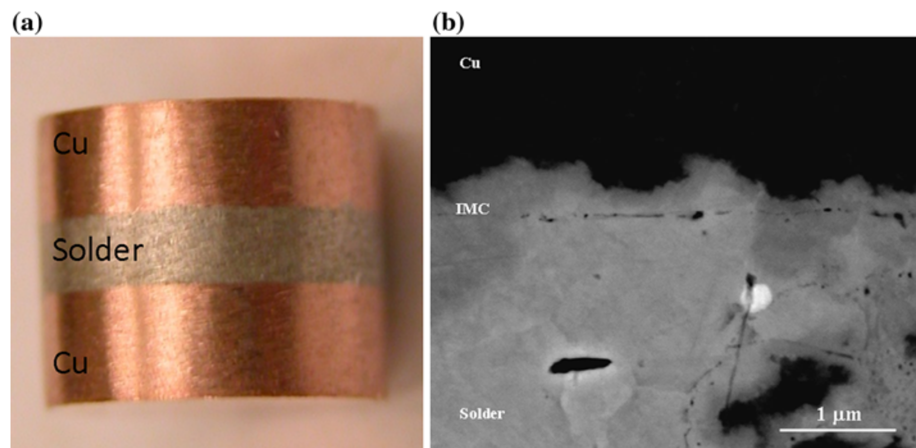

Fig. 15 **a** A photograph of a Cu(Au)-60 vol% In LPS solder joint between two Cu rods and **b** representative SEM micrograph of the interface between Cu and LPS solder. A continuous layer of IMC was formed at the interface proving good chemical bonding between the solder and the Cu substrate

Cu(Au)–In joint. The joint electrical resistance, R_{joint}, is given as:

$$R_{joint} = 2\frac{R_{contact}}{A} + \rho_{solder}\frac{l_{solder}}{A} \quad (12)$$

where $R_{contact}$ is the contact resistance, A is the area of the joint, ρ_{solder} is the electrical resistivity of the solder and l_{solder} is the thickness of the joint. Since the electrical resistivity of the Cu(Au)–In solder is $\sim$1.5 times as of the pure In, the above difference in the joint resistances of Cu(Au)–In and pure In joints suggests that the contact resistance of the Cu/LPS solder interface was similar to that of the Cu/In interface, which is evident from good bonding between Cu and solder (Fig. 15b). Since the electrical and the thermal resistivities of the metallic materials are analogous, it can be concluded from this preliminary work that a joint with Cu(Au)–In LPS solders has superior thermal as well as electrical conductivities as compared to the joints with pure In.

Conclusions

Short-time liquid phase sintering was employed to produce Cu–In-based composite solders for TIM and IC applications. A combination of low sintering temperature, short sintering time, and fast cooling rate produced solders with the highest sintered density. In general, spherical Cu powders exhibited lower compliance as compared to the non-spherical Cu powders. Yield strength as well the thermal conductivity of the composites decreased with an increase in the volume fraction of In; the optimum compromise for TIM and IC applications occurred at 60 vol% of In.

Cu-rich $Cu_{16}In_9$ IMC preferentially formed at the Cu and In interface in the beginning of the liquid phase sintering process. Later, $Cu_{11}In_9$ IMC also formed whose growth rate was very fast, leading to a detrimental effect on the mechanical, thermal, and electrical properties of the Cu–In solders. Coating a thin layer of Au on Cu not only improved the wetting between Cu and In but significantly inhibited the IMC growth by instantaneously forming a continuous tenacious diffusion barrier layer of $AuIn_2$ IMC around Cu particles. In the presence of an Au interfacial layer, only $Cu_{16}In_9$ IMC formed during reflow, at a much slower growth rate than that of $Cu_{11}In_9$. With aging, the $AuIn_2$ layer around Cu particles remained unbroken and effectively inhibited the IMC formation.

Putting an interfacial layer of Au on Cu had an insignificant effect on the yield strength of the as-reflowed solder but significantly improved its thermal conductivity by (i) improving the wetting between Cu and In and (ii) reducing the contact resistance through formation of superior conductive $AuIn_2$ IMC. Consistent with the effect of thermal aging on the growth of the IMC layer at Cu–In and Cu(Au)–In interfaces, the yield strength and the electrical resistivity of the composites containing Au layer increased at a slower rate as compared to the composites without Au layer. With a decrease in the particle size, both the yield strength, and the electrical resistivity of the solder increased.

Acknowledgements This research was supported by a grant from INTEL Corporation through the Strategic Research Segment (SRS) program. Partial support from NSF-CMMI-0709506 and NSF-DMR-0939392 is also acknowledged.

References

1. Dutta I, Raj R, Kumar P, Chen T, Nagaraj CM, Liu J, Renavikar M, Wakharkar V (2009) J Electron Mater 38:2735
2. Liu J, Rottmann P, Dutta S, Kumar P, Raj R, Renavikar M, and Dutta I (2009) In: Proceedings of the 12th electronics packaging technology conference, EPTC, IEEE, Singapore pp 506–511
3. Kumar P, Dutta I, Raj R, Renavikar M, and Wakharkar V (2008) In: Proceeding of conference on thermal issues in emerging technologies (ThETA 2), IEEE, Cairo, pp 339–346
4. Omori M, Takei H (1988) J Mater Sci 23:3744. doi:10.1007/BF00540522
5. Froschauer L, Fulrath RM (1976) J Mater Sci 10:142. doi:10.1007/BF00541086
6. Kingery WD, Niki E, Narasimhan MD (1961) J Am Ceram Soc 44:29
7. Northcutt WG, Ridge O and Snyder WB (1976) US Patent 3,979,234, 7 Sept 1976
8. Wang YP, Zhou L, Zhang MF, Chen XY, Liu JM, Liu ZG (2004) Appl Phys Lett 84:1731
9. Corker DL, Whatmore RW, Ringgaard E, Wolny WW (2000) J Eur Ceram Soc 20:2039
10. German RM, Suri P, Park SJ (2009) J Mater Sci 44:1. doi:10.1007/s10853-008-3008-0
11. Qiao X, Corbin SF (2000) Mater Sci Eng A283:38
12. Palmer MA, Erdman NS, McCall DA (1999) J Electron Mater 28:1189
13. Gallagher C, Matijasevic G and Maguire JF (1997) In: Proceedings of the 54th Electronic Components and Technology Conference (ECTC), San Jose
14. Shearer C, Shearer B, Matijasevic G, Gandhi P (1999) J Electron Mater 28:1319
15. Every AG, Tzou Y, Hasselman DPH, Raj R (1992) Acta Metall Mater 40:123
16. Kim DG, Yoon JW, Lee CY, Jung SB (2003) Mater Trans 44:72
17. Yu SL, Wang SS, Chuang TH (2002) J Electron Mater 31:488
18. Liu HS, Liu XJ, Wang CP, Ohnuma I, Kainuma R, Jin ZP, Ishida K (2002) J Phase Equilib 23:409
19. Pan D, Marks RA, Dutta I, Jadhav S (2004) Rev Sci Instrum 75:5244
20. Miller WS, Humphreys (1991) Scripta Metall Mater 25:33
21. Arsenault RJ, Shi N (1986) Mater Sci Eng 81:175
22. Chawla KK, Metzger M (1972) J Mater Sci 7:34. doi:10.1007/BF00549547
23. Ashby MF (1966) Phil Mag 14:1157
24. Ashby MF (1970) Phil Mag 21:399
25. Sekine H, Chen R (1995) Composites 26:183
26. Simic V, Marinkovic Z (1980) J Less-Common Met 72:133

27. Roy R, Pradhan SK, De M, Sen SK (1993) Thin Solid Films 229:140
28. Rajasekharan TP, Schubert K (1981) Z Metallkd 72:275
29. Jain KC, Ellner M, Schubert K (1972) Z Metallkd 63:456
30. Okamoto H (1993) J Phase Equilib 14:532
31. Liu HS, Cui Y, Ishida K, Jin ZP (2003) J Phase Equilib 27:27
32. Liu YM, Chuang TH (2000) J Electron Mater 29:405
33. Jan JP, Pearson WB (1963) Philos Mag 8:279
34. Nakano T, Suzuki T, Ohnuki N, Baba S (1998) Thin Solid Films 334:192
35. Ma H, Suhling JC (2009) J Mater Sci 44:1141. doi:10.1007/s10853-008-3125-9